DEGREE DESIGN OF COUPLED INFRASTRUCTURES

Abstract. A recent asymptotic model of cascading failure in two-domain, coupled infrastructures is used to pose and solve a specific degree-distribution design problem. Low-order nonlinear analysis exposes the mechanisms by which optimized graphs can form star-like clusters, and suggests why the optimization is well-behaved numerically. Through computational examples on coupled systems of finite size, we demonstrate that the model assumption of degree independence can be somewhat relaxed, which is significant for geometric connectivity. Further, an assortative heuristic rule that matches degrees across the domain boundary can offer benefits in most finite-size cases.

Keywords: interdependent networks; complex systems; asymptotic modeling; cascading failures

1 Introduction

Given the rapid growth of smart distributed systems worldwide, there is great interest among researchers and engineers in the key robustness properties of large-scale and complex systems. Design insights that can be derived from asymptotic descriptions are likely to be important practically, because traditional optimization techniques, and sometimes even simulation, can be intractable at large scales, whereas systems today often grow and reconfigure in real time, and need to have quantifiable robustness. While many papers in the last several decades have provided elegant models and observations of large networks in the natural, social, and technological domains, there are far fewer strong results concerning engineering design at large scales. On one hand, specific motifs which confer robustness have been studied (Newth & Ash, 2007; Gutfraind, 2009), and some guidelines for robust connectivity can be developed for large random graphs, e.g., Paul *et al.* (2006). On the other hand, concerning performance of Internet routers there appears to be little evidence that a purely statistical recipe, applied without domain knowledge, could lead to good designs (Li *et al.*, 2004, 2005). This underscores the gap that exists between practical engineering methods and popular large-scale network descriptions (Alderson & Doyle, 2010, Hines *et al.*, 2010).

Recent work on the cascading failure of coupled infrastructures presents a new opportunity for considering the role of statistical design rules. A control-oriented overview of coupled infrastructures was given by Rinaldi *et al.* (2001), and Newman *et al.* (2005) showed that they are inherently more susceptible to catastrophic failures than systems in a single domain. Use of the z-transform for asymptotic infectious disease outbreak (Newman, 2002) has been recently extended to the case of two coupled graphs (Buldyrev *et al.*, 2010). This work was motivated in particular by studies of Italian power outages in 2003, and the idea of large-scale failures involving interactions between transmission and distributed control systems (Rosato *et al.*, 2008); see also Portante *et al.* (2010) for a description of extremely large failures in the North American grid, which involve both transmission and information systems (Andersson *et al.*, 2005). The model of Buldyrev *et al.* describes a different dynamics than has been

considered elsewhere in the design of large-scale systems, for example cascading failure due to flows exceeding capacities (e.g., Carreras *et al.*, 2002), loss of connectivity in a graph (Ball *et al.*, 1992), Markov chain mixing time (Boyd *et al.*, 2004), and the spread of infection. This makes it an interesting avenue for optimization.

Our first objective in this paper is to use the new asymptotic model to study and solve design problems in degree distribution, for one or both sides in a two-domain infrastructure arrangement. Our second objective is to explore briefly how such designs based on an asymptotic theory can apply to systems with finite size, and having practical constraints such as geometric connectivity. We emphasize that because the model is quite limited in its details, any outcome from optimization should be first interpreted as an early design guide or rule, not a means to specific realizations.

The paper is organized as follows. We describe the model of Buldyrev *et al.* (2010) in Section 2. We frame the main optimization problem of interest, and explore it using a second-order perturbation analysis in Section 3. The perturbation captures accurately all the numerical results obtained with black-box nonlinear optimization tools, and suggests why these tools work well despite the fact that the problem constraints are not convex. It also shows how degree distributions evolve with the mean degree (number of connections), and how clusters appear in the form of strongly bimodal distributions. In Section 4, we then consider design degree distributions when the mean degrees on each side are matched, and when they are different. Moving to finite-size problems in Section 4.3, we design one side's distribution when the distribution of the other side is completely given. In this context, we mention scale effects, consider correlated geometric graphs, and develop a degree-based reordering as a heuristic that takes the role of domain knowledge. These computations are not exhaustive or particularly systematic, but represent the variety of problems that can be tackled. Finally, in Section 5 some concluding remarks are given regarding the implications of our result, and applications.

2 Failure Model and Design Problem

We outline here the procedure for characterizing cascading breakdown in a large, coupled graph structure; this model is due to Buldyrev *et al.* (2010). The domains A and B are both fully connected random graphs, with n nodes each; see Figure 1. A and B are linked together, node-to-node, in normal operation, and then A suffers a random failure in a fraction $1-p$ of its nodes. Rules for the ensuing cascade are as follows: i) the loss of any node destroys all the edges attached to it, within the domain; ii) an A-side node failure induces a B-side failure of the matching node, and vice versa; iii) if an A-node becomes completely disconnected to any other A-nodes, it fails; this is also true on the B-side.

The coupled cascade model tracks giant components on the two sides, employing the z-transform to represent the distribution of node degree $G_{0A}(z,w) = \sum_{m=1}^{\infty} w_m z^m$, on the A-side. The mean degree is $c_A = G_{0A}^{'}(1,w) = \sum m w_m$. The distribution of outgoing degree at a node reached by following a random edge is similarly given by $G_{1A}(z,w) = G_{0A}^{'}(z,w)/c_A$. The giant component fraction following a failure of a fraction $1-p$ of nodes on the A-side is $g_A(z,w) = 1 - G_{0A}(1-p(1-f_A),w)$, where f_A satisfies the implicit relation $f_A = G_{1A}(1-p(1-f_A),w)$ (Shao *et al.*, 2008). If the context is clear, we will drop arguments

when writing G_{0A}, G_{1A}, and g_A. Similar expressions describing the B-side are completely analogous, where we replace w_m with v_n. We denote the size of the giant component, following the initial failure, on the A-side (odd indices) and the B-side (even indices) by μ_i, and define intermediate variables ξ_i. The sequence of operations, as given in the original publication, is as follows: $\mu_1 = pg_A(p)$, $\xi_1 = \mu_1$, $\mu_2 = \xi_1 g_B(\xi_1)$, $\xi_2 = pg_B(\xi_1)$, $\mu_3 = \xi_2 g_A(\xi_2)$, $\xi_3 = pg_A(\xi_2)$, and so on. We drop the subscripts on μ to indicate the fraction still operating on both sides after the cascade has settled.

In our approach, we will minimize the single parameter p that maintains the steady-state giant component $\mu \neq 0$, subject to fixed mean degrees representing cost. Other optimization problems could be developed, for example where the allowable initial loss $1-p$ and terminal giant component size μ are specified, and mean degree becomes a design variable.

3 Analysis

We develop the stated optimization problem in a compact form, for the main purpose of showing the emergence of particular graph structures, as they are encoded into specialized degree distributions. We base our insights on gradient vectors of the objective function, noting this is not a formal analysis of the optimization.

3.1 Linear and Second-Order Approximations

With two different mean degrees on each side, the steady-state condition attained at the end of the cascade is $\xi_{even} = pg_B(pg_A(\xi_{even}))$. More precisely, let q_A and q_B be the arguments to g_A and g_B, respectively, so that $q_B = pg_A(q_A)$ and $q_A = pg_B(q_B)$. As above, we define $g_A(q_A) = 1 - G_{0A}(1 - q_A(1 - f_A))$, where f_A satisfies $f_A = G_{1A}(1 - q_A(1 - f_A))$, and similarly for $g_A(q_A)$ and f_B. Transforming variables such that $r_A = 1 - q_A(1 - f_A)$, the two A-side constraints are

$$\begin{aligned} g_A(q_A) &= 1 - G_{0A} \\ \frac{1 - r_A}{q_A} &= 1 - G_{1A}, \end{aligned}$$

where $G_{0A} = \sum w_m r_A^m$ and $G_{1A} = \sum m w_m r_A^{m-1}$. We similarly define the B-side functions, using v_n and r_B instead of w_m and r_A respectively, and the entire optimization statement is

$$\begin{aligned} \min_{w,\, v,\, q_A,\, q_B,\, r_A,\, r_B,\, p} \quad & p \\ s.t. \quad q_A &= p(1 - G_{0B}) \\ 0 &= (1 - G_{1B})q_B - 1 + r_B \\ q_B &= p(1 - G_{0A}) \\ 0 &= (1 - G_{1A})q_A - 1 + r_A. \end{aligned}$$

For analysis we will essentially adopt a procedure in which w, v are treated separately from r_A, r_B, although all are strictly design variables as written. For a fixed w, v, the broad shape of the minimum p as a function of r_A, r_B can be seen quickly from considering a paired

design in which $w = v$ and therefore $q_A = q_B$ and $r_A = r_B$; collapsing the constraints to one equation, p takes the finite value of $c_A/(c_A - w_1) \geq 1$ at $r_A = 0$, has negative slope there, and then tends to infinity as $r_A \to 1$. Hence, we should expect that the minimum p will come down into the range of $[0, 1]$ for only certain values of r_A (its behavior outside this range is inconsequential). However, a few computations also quickly show that the minimum p is not a convex function of r_A, r_B over $(0, 1) \times (0, 1)$, although it may be quasi-convex. We show an example case below which illustrates these properties, and in particular that for fixed v, w there is a global minimum of p on r_A, r_B, which is easy to find.

We will focus here on the case that w and hence c_A is given, along with c_B, and our task is to optimize v. This is a one-sided design scenario, which has a richness beyond the paired case mentioned above where $w = v$. Also, it is perhaps more realistic than a two-sided case in which only unique c_A and c_B are given, since one domain may be fixed already, or be more constrained than the other. The two-sided setting can be studied using the same methods, however, and both the paired and the two-sided design problems are considered using numerical optimization in a later section.

In this one-sided, non-paired case, then, eliminating q_A and q_B by substitution, we have the simpler constraints

$$\begin{aligned} p(1 - G_{1A})(1 - G_{0B}) - 1 + r_A &= 0 \\ p(1 - G_{1B})(1 - G_{0A}) - 1 + r_B &= 0. \end{aligned} \tag{1}$$

We first derive a key relationship between r_A and r_B. Using the two constraint equations to eliminate p, we find that all of the design variables v, as arguments of G_{0A} and G_{1A}, can be collected on one side of the equation:

$$\frac{(1 - r_A)(1 - G_{0A})}{1 - G_{1A}} = \frac{(1 - r_B)(1 - G_{0B})}{1 - G_{1B}}. \tag{2}$$

Setting $r_a = r_b + \Delta r$ and using the expansion

$$r_A^m = r_A^m + m r_b^{m-1} \Delta r + \left(\begin{array}{c} m \\ 2 \end{array} \right) \Delta r^2 + \cdots$$

we define $G_{0A} = \alpha_0 + \alpha_1 \Delta r + \alpha_2 \Delta r^2 + \cdots$, with

$$\begin{aligned} \alpha_0 &= \sum w_m r_B^m \\ \alpha_1 &= \sum m w_m r_B^{m-1} \\ \alpha_2 &= \sum \left(\begin{array}{c} m \\ 2 \end{array} \right) w_m r_B^{m-2} \\ &\cdots \end{aligned}$$

We make a similar expansion $G_{1A} = \beta_0 + \beta_1 \Delta r + \beta_2 \Delta r^2 + \cdots$, with

$$\begin{aligned} \beta_0 &= \frac{1}{c_A} \sum m w_m r_B^{m-1} \\ \beta_1 &= \frac{1}{c_A} \sum m(m-1) w_m r_B^{m-2} \\ \beta_2 &= \frac{1}{c_A} \sum m \left(\begin{array}{c} m-1 \\ 2 \end{array} \right) w_m r_B^{m-3} \\ &\cdots \end{aligned}$$

The A-side of Equation 2, with these expansions inserted, has a linearization of the form $\phi + \psi\Delta r$, where

$$\begin{aligned} \gamma &= 1 - r_B \\ \phi &= \frac{\gamma(1-\alpha_0)}{1-\beta_0} \\ \psi &= \frac{\beta_1\phi + \alpha_0 - \alpha_1\gamma - 1}{1-\beta_0}. \end{aligned}$$

In sequence, we truncated the higher order terms in $1-G_{0A}$ and $1-G_{1A}$, invoked $1/(1-\epsilon) \approx 1+\epsilon$ for $|\epsilon| << 1$, and then eliminated higher-order products. Critically, this linearization does not require any information from the B-side fraction in Equation 2. The linearization is good for all the design problems we have studied, and can be justified in detail by inserting specific numbers; it is is easily accurate to a few percent.

Now we connect Δr with the B-domain design problem. Let $y = 1-G_{0B}$ and $z = 1-G_{1B}$. Equation 2 implies the approximation

$$\Delta r \approx \frac{\gamma y - \phi z}{\psi z},$$

which can now be used to characterize p in the original constraint equation pair. We will employ Equation 1, since r_A appears only once:

$$pz(1 - \alpha_0 - \alpha_1\Delta r - \alpha_2\Delta r^2 - \cdots) - 1 + r_B = 0. \tag{3}$$

Proceeding for the moment with the first-order term only, we obtain

$$-\frac{\alpha_1}{\psi}y + \frac{1}{\gamma}\left(1 - \alpha_0 + \frac{\alpha_1\phi}{\psi}\right)z \approx \frac{1}{p}.$$

This is significant because (for a given r_B) minimizing p is the same as maximizing $1/p$, and the left side of the equation is linear in the design variables v – they only appear in y and z. To express derivatives of y and z with respect to an element v_n, we use the fact that $\sum v_n = 1$ and $\sum nv_n = c_B$ to first remove v_1 and v_2 from consideration; we have

$$\begin{aligned} v_1 &= 2 - c_b + v_3 + 2v_4 + \cdots \text{ and} \\ v_2 &= c_b - 1 - 2v_3 - 3v_4 - \cdots. \end{aligned} \tag{4}$$

These augment the constraints that $0 \le v_n \le 1$, and we can now write for $n \ge 3$

$$\begin{aligned} \frac{dy}{dv_n} &= -(n-2)r_B + (n-1)r_B^2 - r_B^n \\ \frac{dz}{dv_n} &= \frac{1}{c_B}\left(-(n-2) + 2(n-1)r_B - nr_B^{n-1}\right). \end{aligned}$$

Note that both of these are functions only of c_B and r_B. Thus, for a given r_B, finding the optimum design v is essentially a small linear program, and the cost of sweeping through r_B to find the minimum p is negligible.

Numerical solutions to the original problem occur at locations other than the vertices of the polytope, however, belying the importance of the second-order α_2 term in our treatment of Equation 3. Working through the algebra, we have the more accurate form

$$\begin{aligned}
\frac{1}{p} &\approx \delta_1 y + \delta_2 z + \delta_3 \frac{y^2}{z}, \text{ where} \\
\delta_1 &= -\frac{\alpha_1}{\psi} + \frac{2\alpha_2\phi}{\psi^2} \\
\delta_2 &= \frac{1-\alpha_0}{\gamma} + \frac{\alpha_1\phi}{\gamma\psi} - \frac{\alpha_2\phi^2}{\gamma\psi^2} \\
\delta_3 &= -\frac{\alpha_2\gamma}{\psi^2}.
\end{aligned}$$

Combining terms, we obtain

$$\frac{d}{dv_n}\left(\frac{1}{p}\right) = \left(\delta_1 + \delta_3\frac{2y}{z}\right)\frac{dy}{dv_n} + \left(\delta_2 - \delta_3\frac{y^2}{z^2}\right)\frac{dz}{dv_n}, \tag{5}$$

where the derivatives of y and z are as before. The nonlinear effects are shown in the $2y/z$ and y^2/z^2 terms multiplying δ_3. Finding v given r_B is no longer a linear program.

3.2 Behavior of the Approximate Solutions

We address here and in our later sections the case of $c_B = 2.5$, a fairly low connectivity specification and therefore a challenging constraint with which to develop robustness. The feasible set of solutions up to v_5 is given in Figure 2. On the A-side, we consider regular graphs of mean degree between 2.5 and 5.5 (we refer to fractional regular graphs with the understanding that only one, or two consecutive, nonzero degree probabilities are possible, and they scale so as to ensure the mean degree). For each c_A, we scan through r_B as needed, and compute the gradient of $1/p$ with the design variables as described above. For linear analysis, the gradient depends only on r_B and not on v. We also plot gradients obtained from the second-order analysis; in this case they depend on both r_B and v. In our drawings on the feasible polytope, the gradient magnitude across all designs v is normalized, and sometimes these vectors are uniformly rescaled with respect to the polytope, to help visibility. Along with the gradient vector, we plot its projection on the active face. Finally, when we list a specific degree distribution v, unspecified values are implied zero, e.g., $[v_3 = 1/5, v_4 = 4/5]$ is a complete description. Typical calculations in Δr and p are shown in Figure 3, confirming that p is a well-formed curve (although not convex) for the family of designs studied, and that Δr is small.

The case of $c_A = 2.5$ is described first. Linear analysis gives the gradient as shown in Figure 4. It is negative in all three directions, and the point $v_3 = 1/2$ on the plot is the optimum, inducing $v_2 = 1/2$ by Equation 5. This makes B a 2.5-regular graph, and hence the A and B sides are paired. We find for this case that gradients from the nonlinear analysis are indistinguishable from the linear, and so are not shown.

Next we consider $c_A = 3.5$, in Figure 5. The optimum is at the point $v_3 = 3/4$, inducing $v_1 = 1/4$. This is our first evidence of a more complex structure coming from the

optimization, even based on the linear analysis. We refer to this as a "split" or bimodal design, wherein no degree-two nodes occur, and (as we will show) only v_1 and one or two other v_n are nonzero. In the second-order case, shown in Figure 5 (right), the optimum point comes out to be the same, but the information in the gradients is much more complex. First, on the inner face, gradients are pointed away and upward from the origin, while on the outer face, they point inward and down as for the linear model. On both faces, however, there is a component towards the point $v_3 = 3/4$; at this location, the gradient is significantly deflected so as to point nearly in the direction $[1, 1, 0]$.

An examination of the second-order effects in Equation 5 shows that they become important through several mechanisms, illustrated in Figure 6. First, δ_3 is always negative and y/z is always positive, and therefore an offset occurs to δ_1, which is always positive. δ_2 can be positive or negative, and small in magnitude; in this case it is dominated by the δ_3 term. For the specific setting of $c_A = 3.5$ in the figure, we find in the neighborhood of minimum p ($r_B \approx 0.52$) that $\delta_1 \approx 2.7$, $\delta_2 \approx -0.1$, and $\delta_3 \approx -0.9$. With y/z in the range of 0.9–1.3 over all the designs v, the term multiplying dz/dv_n in Equation 5 is indeed dominated by the $\delta_3 y^2/z^2$ part, and can vary by a factor of about two. The term multiplying dy/dv_n in Equation 5 has a similar, two-fold variation over v because of sign cancelation. Both of these terms multiplying dy/dv_n and dz/dv_n are positive. We see further that dy/dv_n itself is negative, while dz/dv_n is positive near $r_B = 0.52$, for $c_A = 3.5$. Thus a further cancelation effect occurs, and by now it is clear that the derivatives of $1/p$ can be very substantially controlled by the second-order effects. We shall not attempt a more fundamental assessment than this here.

Resulting from these properties, the transition from the vertex solution for $c_A = 2.5$ and that for $c_A = 3.5$ cannot be accurately captured with the linear analysis, but is seen clearly for $c_A = 3.1$ in Figure 7, with the nonlinear effects added. Here the gradient at $v_3 = 1/2$ (inner face) drives the optimum outward on the v_3 axis, while at $v_3 = 3/4$ (outer face) the gradient drives it back. Although not evident in the plot, the line segment on the v_3 axis is active. Hence, we have identified an intermediate solution on this segment with $1/2 \le v_3 \le 3/4$, over which range v_1 and v_2 exchange roles.

As we increase c_A further, the linear analysis becomes worse, in the sense that even vertex optima are not necessarily indicated clearly. For example, with $c_A = 4.5$, the apparent optimum with nonlinear analysis is $v_4 = 1/2$, inducing $v_1 = 1/2$. The linear analysis instead puts the optimum at $v_5 = 3/8$; this occurs because the projection on the outer plane has an incorrect, slight positive vertical component. These observations are based on Figure 8.

As with c_A near 3.0, there exists a continuous transition between the two vertex solutions for $c_A = 3.5$ and $c_A = 4.5$. This is identified using the nonlinear analysis for $c_A = 3.9$ in Figure 9. Along the lower edge of the outer plane, the gradient at the midpoint v has a component to the right in the figure, towards the vertex $v_4 = 1/2$, while the gradient at the next v on this edge has a component in the opposite direction, towards the vertex at $v_3 = 3/4$.

The transition from $c_A = 4.5$ to 5.5 is similar. The linear analysis gives the optimum at $v_5 = 3/8$ for $c_A \ge 4.5$; however, we have not allowed the solution to move into v_6, so it is unclear where the linear gradient will drive it at $c_A = 5.5$. The nonlinear analysis again gives a mid-edge solution, between $v_4 = 1/2$ and $v_5 = 3/8$, for c_A near 5.0; for $c_A = 5.5$ we have $v_5 = 3/8$, and can expect that v_6 will become active shortly.

Summarizing, for each c_A the gradients shown indicate a unique solution that can be found by a nonlinear optimization algorithm. From the linear (L) and nonlinear (NL) analysis we have (with $c_B = 2.5$ and A a c_A-regular graph):

c_A	2.5	3.0	3.5	4.0	4.5	5.0	5.5
L	$v_3 = 1/2$	$v_3 = 1/2$	$v_3 = 3/4$	$v_4 = 1/2$	$v_5 = 3/8$	$v_5 = 3/8$	?
NL	$v_3 = 1/2$	on edge	$v_3 = 3/4$	on edge	$v_4 = 1/2$	on edge	$v_5 = 3/8$

A property shared by both the linear and nonlinear models is that nodes of degree two are never in the solution v, except at the lowest c_A value. This is synonymous with the solutions traveling along the marked paths on the outer plane in Figure 2. We refer to these broadly as split designs, where only a few elements of v are active: v_1, and one or two others for which $n \approx c_A$. We find in the next section that split distributions are ubiquitous in this optimization problem.

4 Numerical Optimization

Our next objective is to carry out the optimization described above for some different application types, to develop further properties of the solutions, and to assess strengths and limitations of this approach. We consider below separate design scenarios in which i) the mean degree for both sides is the same and fixed (paired case; $c_A = c_B$ given, design $w = v$), ii) the mean degrees are distinct and fixed (two-sided, non-paired; $c_A \neq c_B$ given, design $w \neq v$), and iii) the mean degrees are fixed and possibly distinct, and the distribution on one side is completely defined (one-sided, non-paired; c_A, c_B, and w given, design v). We apply a standard constrained nonlinear optimization using the active-set method in all of our computations, and use the notation p^* to indicate the minimum value of p found.

4.1 Two-Sides Design with Matched Mean Degrees

The first obvious case is $c_A = c_B = 2.4554 \equiv \gamma_{ER}$, which was considered by Buldyrev *et al.* (2010), for Erdős-Rényi graphs. Our optimization yields $p^* = 0.913$, leading to a final giant component fraction of 0.811. This means that the system will survive an initial loss of about nine percent of nodes on the A-side, and in this case, the system ultimately loses about twenty percent of its functionality. The designed distribution is simple: $w_2 = 0.545$ and $w_3 = 0.455$, so the optimization has created a matched pair of γ_{ER}-regular graphs. This first result is not unexpected, since a pair of ER graphs would be hard to defend as an optimized form according to any operational metric. At the same time, it is striking because the designed distribution is a net zero-cost rewiring of the ER network that allows the coupled structure to move from essentially zero robustness to a nine percent loss.

Among the entire family of optimum designs for different mean degree specifications, as expected p^* decreases as c_A increases: highly-connected graphs are more robust. Table 1 shows the product $p^* c_A$, which serves as a simple performance metric relative to the ER case, for different settings of c_A; p^* being low captures robustness, whereas c_A scales the cost. All of the designed distributions are regular, so the graph with $c_A = 2.1$ has a chain-

like structure, with occasional degree-three nodes. The advantages of the design are greatest relative to the ER case at the lower mean degree. Table 2 shows the ultimate system size fraction μ for $c_A = [3, 4]$, at different levels of initial failure. As expected, it is only near the critical failure level that the final GC sizes are substantially below the initial failure size, and therefore the ultimate loss level increases gracefully with increasing initial damage.

4.2 Two-Sides Design with Different Mean Degrees

As would be expected, the two-sides scenario shows a richness that is not evident when the mean degrees are constrained to be the same. However, it recovers exactly the scenario developed in the perturbation study for $c_B = 2.5$; the higher-degree side (A) takes a regular distribution, whereas the lower-degree side takes a split form. In none of these cases are nodes with degree two expressed in v. One explanation is simply that degree-two nodes are three times as expensive as are degree-one nodes, in terms of contributing to the low mean degree of $c_B = 2.5$ that we enforce, but they are only twice as robust, in terms of the number of original in-domain connections. By this reasoning, local star-like structures would always be preferred on the B-side. On the A-side, the regular form which emerges can perhaps be motivated from the fact that paired regular graphs are preferred when the mean degrees are equal.

4.3 One-Side Design with Different Mean Degrees

We now consider the case where w is given, and the task is to design v, given c_B. This is the same scenario as in the perturbation analysis, but here we will broaden our view significantly. The previous sections employed only the asymptotic model; here, we attempt a much closer connection with applications by considering finite sizes and several important graph types. For each, we will i) create a realization for one side, with size $N = 1000$, and compute its degree distribution, ii) design the distribution of the second side, iii) generate a size $N = 1000$ realization of the second side, and iv) study the behavior of the aggregate system using the explicit cascading process on which the asymptotic model is based. We have verified our full model against the results in Buldyrev *et al.* (2010), to the extent possible given our fairly small network size. We consider mainly the case of $N = 1000$ because our purpose is not to study scaling effects relative to the asymptotic model, as has been done already elsewhere; rather this size of system is between the scales at which deterministic design strategies could be employed, and the scales at which an asymptotic description should be accurate.

In Table 3, we give critical p-values from ensembles in which half of the members suffer a complete cascading failure, and the other half do not. We define a complete failure somewhat arbitrarily as the result that the giant component is less than ten percent of p. It is important to note that in the table p is not interpreted as a design variable any more, but as one minus the actual failure size imposed at the beginning of each trial. Each ensemble has one thousand trials.

4.3.1 Definition of Graph Types and a Heuristic

The upper portion of the table shows results for pairings of some standard graphs, and introduces several graphs that we will consider specifically as a basis for design in the next subsection. As is well known, regular graphs are robust against random failures in one domain; this is seen again in the multi-domain case, where for $c_A = c_B = 4$, over forty percent of nodes on one side can be eliminated without leading to total collapse; this is in agreement with the asymptotic result in Table 1. A 4-regular graph paired with a scale-free preferential attachment graph of equal mean degree has a similar robustness level; our scale-free preferential attachment graphs (SFPA) (Barabasi & Albert, 1999) have slope $\gamma = 3$ and mean degree four. When degree heterogeneity appears on both sides, we can expect that the correlation across the domain boundary matters. We therefore introduce an assortativity-like heuristic to the realization, in the ordering of nodes: our "inverse" configuration in the table reorders the boundary connections so that high-degree nodes on one side are connected with low-degree nodes on the other; our "matched" configuration connects high-degree nodes on both sides together. The table shows that paired ER and paired SFPA graphs having matched connections are substantially more robust than those with random or inverse connections. These properties are obviously dependent on scale, because we implement reordering in the realization.

We also generate "hybrid geometric" scale-free (hgSFPA) graphs wherein the preferential attachment recipe is augmented by the distance between nodes, so that long-distance links are made rarer, while short-distance links are more common. The probability of connecting an existing node u with a new node v is taken in the hgSFPA as $P(u \sim v) = k_u/d_{uv}^4$, subject to a normalization factor, where k_u is the degree of node u and d_{uv} is the geometric distance between the nodes. Such geometric preference is a ubiquitous property of real-world systems operating in the spatial domain, and correlates the degree distribution. As one measure of this structure, our hgSFPA has a clustering coefficient of about 0.3. The graph has a non-power-law degree distribution, but maintains the mean degree four; see Figure 10 for a typical realization with $N = 1000$. In Table 3, we see that a pairing of hgSFPA graphs is not as robust as the ER and SFPA pairs.

We finally generate formal geometric graphs (Penrose, 2006). In this case, connections are made solely on the geographic separation of points; if the distance is within a fixed threshold they are connected with probability one. A typical geometric graph for our study is shown in Figure 10; it has mean degree 8.8 and clustering coefficient about 0.6. In Table 3, there is virtually no effect of making reconnections based on degree between two such paired geometric graphs, a consequence of the very high dependence among node degrees. The critical value of p is good primarily because the mean degree is so much higher than in the other cases discussed so far.

4.3.2 One-Side Design Results

Next we undertake the design of degree distributions on one side, given the distribution of the other. These computations use the specific graph types outlined above, and with the same specifications of mean degree and γ. We will assume as before that the mean degree on the side to be designed is 2.5, corresponding with fairly low connectivity, and that the mean

degree of the other side is higher. Now the side on which initial failures occur is important for finite-size systems, if the properties of the two sides are different. Intuitively, removing a fraction of nodes in a low-connectivity random graph could be markedly more damaging than in a high-connectivity setting. Thus, in accordance with the convention that the asymptotic model specifies initial failures on the A-side, *in the rest of our computations we design and damage the A-side.*

The first case has B given as a 4-SFPA graph. Here the optimal design for A is a simple 1-4 split, i.e., $w_1 = w_4 = 1/2$, as shown in Figure 11. As the maximum degree m_{max} increases, representing wider and wider splits, p^* increases to unity, indicating a loss of robustness; at m_{max} 25 in this example, the system tolerates no failures at all ($p^* = 1$). This is a condition where the optimization problem has no non-trivial solution. It is noteworthy also that the giant component fraction μ generally degrades as m_{max} and p^* increase.

Considering now the finite-size results for the optimal 1-4 split, robustness is dramatically improved by ordering the connections – the inverse, random, and matched connections confer robustness levels of about 10%, 20%, and 30% losses respectively in Table 3. We have also given the results for a suboptimal 1-8 split and a 2.5-regular graph; the probability of the giant component is shown versus the initial loss size for all three cases in Figure 12 (left). The 1-8 split is more robust overall than the optimal 1-4 split, and broadly speaking this disparity is a result of finite size, as illustrated in Figure 12 (right) for random ordering. Such scaling effects can be appreciated at a fundamental level by the fact that the asymptotic model has nothing to say about star networks, and yet with any finite-size graph, $g_A(p) = 1$ with probability p, and $g_A(p) = 0$ with probability $1 - p$. In other words, in a star there are no giant component calculations to do on the A-side – either the hub is hit or not. For the present case, expanding N ("L" entries in the table) significantly reduces the relative improvements of the 1-8 split for random ordering, as might be expected. With matched ordering, we find that the 1-8 split offers an extraordinary robustness level; this outcome is certainly a scale effect also, but it is a larger question and outside our scope here.

Next we apply the design procedure with B a 4-hgSFPA. Although the maximum degree in B can be quite high (perhaps thirty for $N = 1000$), the same optimum solution $w_1 = w_4 = 1/2$ emerges again for $c_A = 2.5$. The matched ordering creates a very substantial robustness level, given the obvious geometric structure in Figure 10. Again, the suboptimal 1-8 split is superior for $N = 1000$, and especially for matched ordering.

The table next shows results when B is an 8.8-ER graph, as a transition from the well-performing designs at lower levels of c_B to the formal geometric graph with $c_B = 8.8$. The 1-8 split with $w_1 = 11/14, w_8 = 3/14$ is optimal, and as expected with high connectivity the robustness is good. The 1-12 split offers minor enhancements at this scale. Finally, we consider the random geometric graph on the B-side. Since we showed for a pair of these geometric graphs that reordering has little effect on robustness, we expect and see a similar insensitivity here. Nevertheless, again the split designs are better than the regular graph, and ordering can offer a minor improvement with the 1-12 split, subject to scale.

5 Discussion

This study has identified a new optimization problem for the robust design of very large two-domain systems, built upon a recent asymptotic model of Buldyrev *et al.* (2010). A second-order perturbation analysis gives insights as to why the problems are reasonable to solve with generic tools, and is sufficient to bring out some key attributes of the solutions, which we further develop with numerical optimizations. Most notably, split, or bimodal, degree distributions arise; these are associated with hub-and-spoke topologies, which are of course well-known and have been discussed in other works on network robustness, e.g., Tanizawa *et al.* (2005). We verified system robustness properties with non-asymptotic, finite-size cascading failure simulations, subject to scaling effects. An added heuristic step of reordering the cross-domain connections according to their degree adds some improvements.

The asymptotic model employed here was motivated in the context of a controlled power system (Rosato *et al.*, 2008). The model will shut down a control node when its paired generator or load substation fails, and conversely shut down a substation when its control node fails. The model further eliminates the in-domain edges connected to failed nodes, so that the loss of a node also removes any role its site may have had as a power bus or a data router. In the general context of spreading infection, in-domain edge losses are quite plausible if failures create transient events – such as surges, latency, or bad packets – that can propagate. Although the model is a worst-case scenario, similar analogies could be made for many systems in which one side is a flow network and the other a communication and control grid. Another major manifestation of coupled infrastructures is a group of coordinated agents performing an integrated task and operating in a physical domain. That such distributed systems will constitute infrastructure in the future seems unavoidable. Consider as one example a collaborative localization mission with underwater, mobile robotic sensors (Bahr *et al.*, 2009). Communications and navigation underwater employ the acoustic channel, which brings serious reliability, range, and capacity constraints in comparison with the wireless links available in most terrestrial and air scenarios (Sozer *et al.*, 2000, Stojanovich, 2006). For vehicles performing relative localization with each other, A-side edges represent relative positioning constraints and B-side edges the communication network; it is often the case that ranging packets are not used for data transmission. Thus, if a first vehicle loses communication with the other agents, it will not be able to maintain its relative position as easily, since it cannot know the velocities, absolute positions, or intents, of the others. Vehicles that were depending on the first for their own positioning will in turn have their navigation compromised, and could drift out of communication range. In short, both the communication and navigation links need to function for the system to work. Practically speaking, marine operational challenges derive not only from the acoustic channel, but also from ocean currents and waves, shipping traffic, and underwater fouling, all of which are real hazards to autonomous vehicles.

Because our approach is rapid but lacks many details in the modeling as described, it is primarily useful for early design concepts, or fast reconfiguration of distributed systems. Considering the topology of a fixed power grid, for example, the procedure establishes a relationship between allowable initial failure size $1 - p$ and the required mean degree, which reflects the installation cost. Specific realizations that match the desired degree distribution, and respect the main assumptions, should have an inherent robust structure, which can be

fine-tuned using more domain-specific tools. This is a common strategy, for example, in the use relaxations of nonlinear programs: the solution may not be feasible as given, but important elements of the optimal feasible solution are revealed. For active reconfiguring of large systems such as groups of mobile agents, our approach can shape *real-time* degree distributions that trade off robustness with other properties such as diameter, possibly modifying the mean degree as needed on the fly. If small perturbations are expected, then there is no need to operate with a high mean degree.

More broadly, the roles of detailed versus statistical optimization in large-scale systems have been argued in several contexts, and robustness very likely requires specificity in design. Nevertheless as we have shown, in the case of a two-domain dynamics the emergent statistical character – the split degree design specifically – measurably affects robustness of the system. For any 1-m_{max} split design, all the edges are either m_{max}-to-m_{max} in their node degrees, or 1-to-m_{max}. We cannot create edges of node degrees 1-to-1, so all the realizations have equal relative likelihood (Li *et al.*, 2004). This does not mean, of course, that all rewirings have equal performance or robustness, but, critically, that there are fewer to work with. In this sense our asymptotic optimization process has significantly reduced the space of design solutions (Bianconi, 2008). A simple example illustrates the constraints provided by the split designs. A 2.5-regular graph with eight nodes has at least twenty-five unique connections (to isomorphism), and a twelve-node version has more than 1300; these are estimated by comparing the adjacency spectra of many random realizations. Consider now the 1-8 split with $c_A = 2.5$, as in our numerical experiments; $w_1 = 11/14$ and $w_8 = 3/14$. A fourteen-node realization is impossible, because the number of half edges is odd; but a twenty-eight node realization can be hooked up in exactly two ways, as shown in Figure 13.

Considering future work, the major assumptions made in the asymptotic model are that the random graphs on either side are themselves uncorrelated and have local treelike structure, that there is a one-to-one nodal interconnection between the two graphs, and that successive, coupled node and edge failures occur in the manner described. Scale-free and ER graphs have the first property, but in fact a number of more specialized graphs could be accommodated formally, including those with degree correlations (Newman, 2002). Our design example with geometrically-correlated graphs also suggests that effective designs can be applied even when the assumptions are not strictly met. Relevant to the second assumption, very recent work has extended the model to allow fully in-domain nodes (Parshani *et al.*, 2010); design optimization within this new framework would be an interesting direction of inquiry. Finally, the case of targeted attacks, for example where the most highly-connected nodes are destroyed, is of high interest and would complement the present study.

References

Alderson, D.L., and J.C. Doyle (2010), Contrasting views of complexity and their implications for network-centric infrastructures, *IEEE Trans. Systems, Man, and Cybernetics: A Systems and Humans*, 40(4), 839-52.

Andersson, G., P. Donalek, R. Farmer, N. Hatziargyriou, I. Kamwa, P. Kundur, N. Martins, J. Paserba, P. Pourbeik, J. Sanchez-Gasca, R. Schulz, A. Stankovic, C. Taylor, and V. Vittal (2005), Causes of the 2003 major blackouts in North America and Europe, and recommended means to improve system dynamic performance, *IEEE Trans. Power Systems*, 20(4),1922-8.

Bahr, A., J.J. Leonard, and M.F. Fallon (2009), Cooperative localization for autonomous underwater vehicles, *Int. J. Robotics Research*, 28(6), 714-28.

Ball, M.O., C.J. Colbourn, and J.S. Provan (1992), Network reliability, University of Maryland Technical Research Report TR92-74.

Barabasi, A.L. and R. Albert (1999), Emergence of scaling in random networks, *Science*, 286(5439), 509-12.

Bianconi, G. (2008), The entropy of randomized network ensembles, EPL, 81, 28005.

Boyd, S., P. Diaconis, and L. Xiao (2004), Fastest mixing Markov chain on a graph, *SIAM Rev.*, 46(4), 667-89.

Buldyrev, S.V., R. Parshani, G. Paul, H.E. Stanley, and S. Havlin (2010), Catastrophic cascade failures in interdependent networks. *Nature* 464(15), 1025-8.

Carreras, B.A., V.E. Lynch, I. Dobson, and D.E. Newman (2002), Critical points and transitions in an electric power transmission model for cascading failure blackouts, *Chaos*, 12(4), 985-94.

Gutfraind, A. (2009), Constructing networks for cascade resilience, arXiv:0906.0786.

Hines, P., E. Cotilla-Sanchez, and S. Blumsack (2010), Do topological models provide good information about electricity infrastructure vulnerability? *Chaos*, 20(3) 033122.

Li, L., D. Alderson, W. Willinger, and J. Doyle (2004), A first-principles approach to understanding the Internet's router-level topology. *Proc. SIGCOMM'04*, Portland, OR.

Li, L., D. Alderson, J.C. Doyle, and W. Willinger (2005), Towards a theory of scale-free graphs: Definition, properties, and implications, *Internet Mathematics*, 2(4), 431-523.

Newman, M.E.J. (2002), Spread of epidemic disease on networks, *Phys. Rev. E*, 66, 016128.

Newman, D.E., B. Nkei, B.A. Carreras, I. Dobson, V.E. Lynch, and P. Gradney (2005), Risk assessment in complex interacting infrastructure systems, *Proc. 38th Hawaii Int. Conf. on System Sciences*.

Newth, D., and J. Ash (2007), Optimizing complex networks for resilience against cascading failure. *Physica A*, 380, 673-83.

Paul, G., S. Sreenivasan, S. Havlin, and H.E. Stanley (2006), Optimization of network ro-

bustness to random breakdowns, *Physica A*, 370, 854-62.

Parshani, R., S.V. Buldyrev, and S. Havlin (2010), Interdependent networks: Reducing the coupling strength leads to a change from a first to second order percolation transition, *Phys. Rev. Letters*, 105, 048701.

Penrose, M. (2009), Random geometric graphs. Springer.

Portante, E.C., J.A. Kavicky, S.F. Folga, B.A. Craig, and Leah E. Talaber (2010), Simulating the impacts of a New Madrid earthquake on the regional electric infrastructure, *Proc. Summer Computer Simulation Conf.*, Ottawa.

Rinaldi, S.M., J.P. Peerenboom, and T.K. Kelly (2001), Identifying, understanding, and analyzing critical structure interdependencies, *IEEE Control Systems Magazine*, 11-25, December issue.

Rosato, V., L. Issacharoff, and F. Tiriticco, S. Meloni, S. de Porcellinis, and R. Setola (2008), Modeling interdependent infrastructures using interacting dynamic models. *Int. J. Critical Infrastructures*, 4(1/2), 63-79.

Shao, J., S.V. Buldyrev, R. Cohen, M. Kitsak, S. Havlin, and H.E. Stanley (2008), Fractal boundaries of complex networks. *Europhysics Letters* (84) 48004.

Sozer, E.M., M. Stojanovich, and J. Proakis (2000), Acoustic underwater networks. *IEEE J. Oceanic Engineering*, 25(1), 72-83.

Stojanovich, M. (2006), On the relationship between capacity and distance in an underwater acoustic communication channel, *Mobile Computing and Communications Rev.*, 11(4), 34-43.

Tanizawa, T., G. Paul, R. Cohen, S. Havlin, and H. E. Stanley (2005), Optimization of network robustness to waves of targeted and random attacks, *Phys. Rev. E*, 71, 047101.

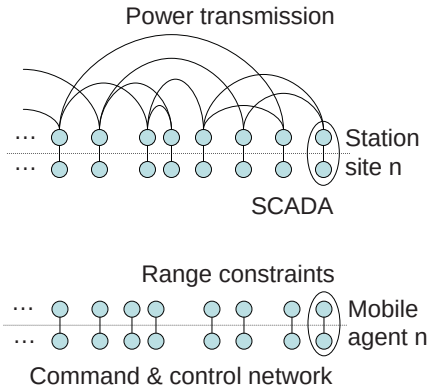

Figure 1: Two-layer coupled network examples, in a power system and for a group of autonomous vehicles with collaborative navigation. For clarity, edges are drawn only for the transmission side of the power system.

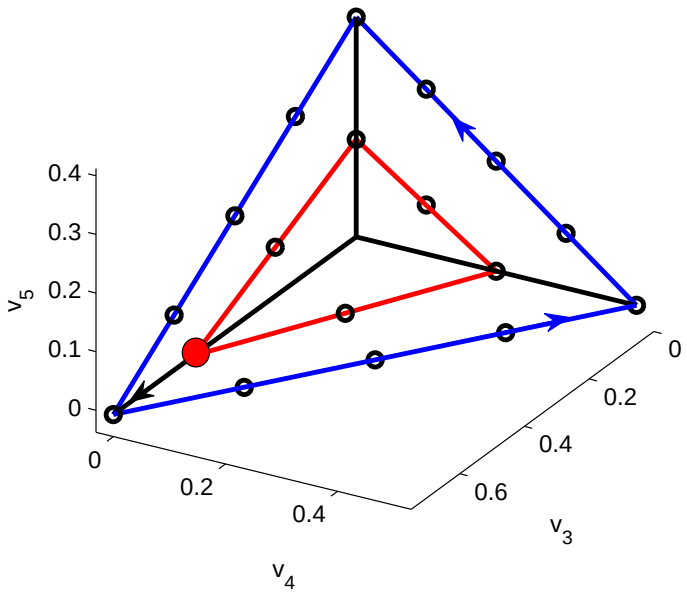

Figure 2: With $c_B = 2.5$ given and v_1, v_2 given by Equation 4, the feasible set for v_3, v_4, and v_5 is the polytope defined by the inner red plane and the outer blue plane, bounded by $v_3 \geq 0$, $v_4 \geq 0$, and $v_5 \geq 0$. The planes are not parallel. At $c_A = 2.5$ and $c_B = 2.5$, the optimal v to minimize p is the red dot, $v_3 = 1/2$. As c_B increases to 5.5, solutions move along the boundaries indicated with arrows. Black circles indicate the specific designs v where we make gradient calculations.

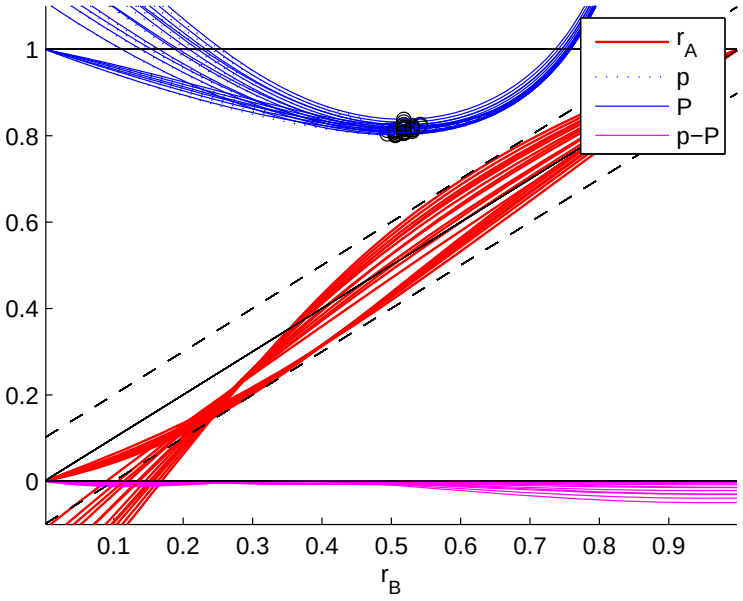

Figure 3: Typical calculations for the case of $c_A = 3.5$. The curves represent all of the eighteen design points in Figure 2. Δr takes values on the order of 0.1 or less; the p shown is based on the keeping α_1 in Equation 3, while the second-order equivalent is labeled P. The minimal p are found over a narrow set of r_B, as indicated by the overlaid circles.

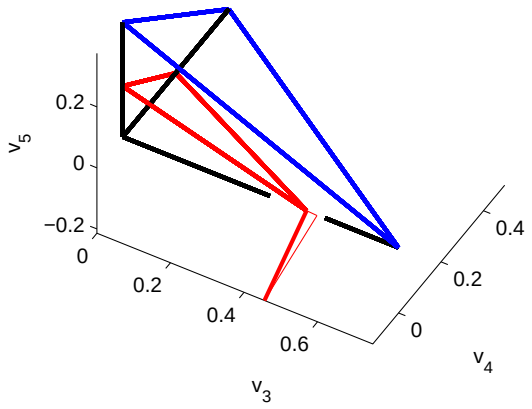

Figure 4: The linear gradient (protruding bold) and its projection on the active plane at the optimal vertex, for $c_A = 2.5$.

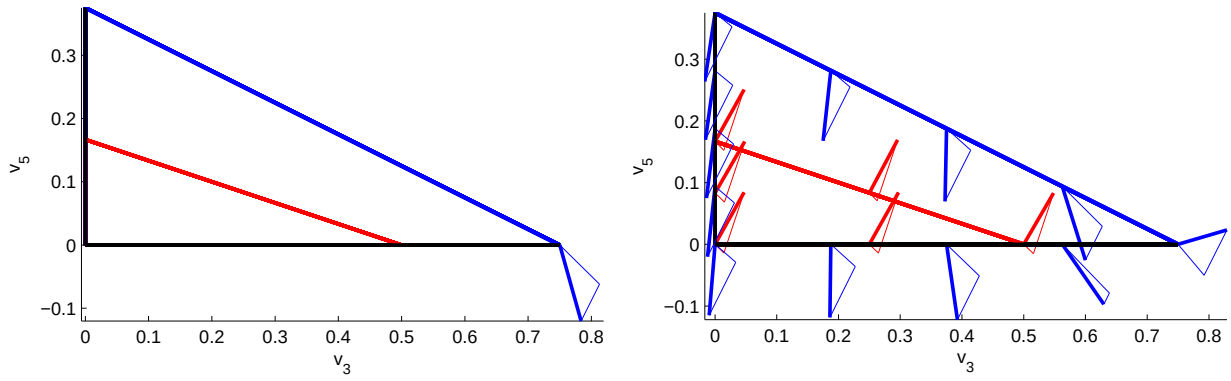

Figure 5: The linear (left) and nonlinear (right) gradients and their projections onto the active planes, for $c_A = 3.5$. The polytope is viewed from the along the negative v_4-axis.

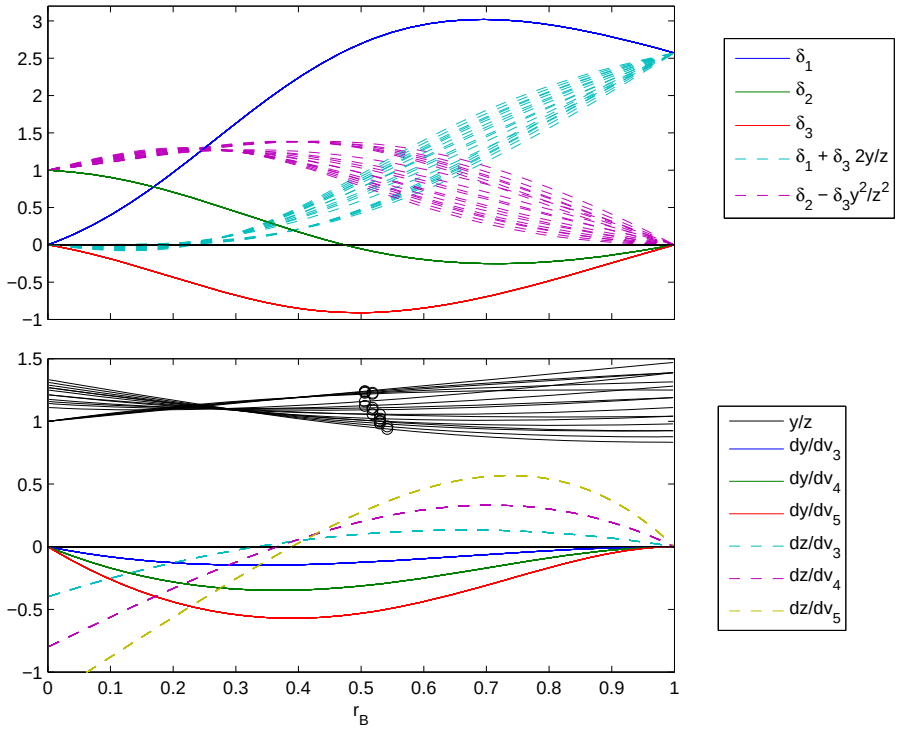

Figure 6: Terms appearing in the second-order expansion for gradients of $1/p$ with v_n, and $c_A = 3.5$. The circles overlaid on y/z indicate locations of minimum p across the eighteen designs considered.

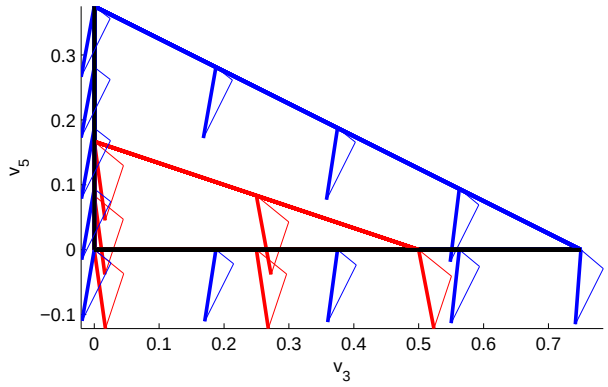

Figure 7: Gradients from the nonlinear analysis, and their projections, for $c_A = 3.1$. The polytope is viewed from along the negative v_4-axis.

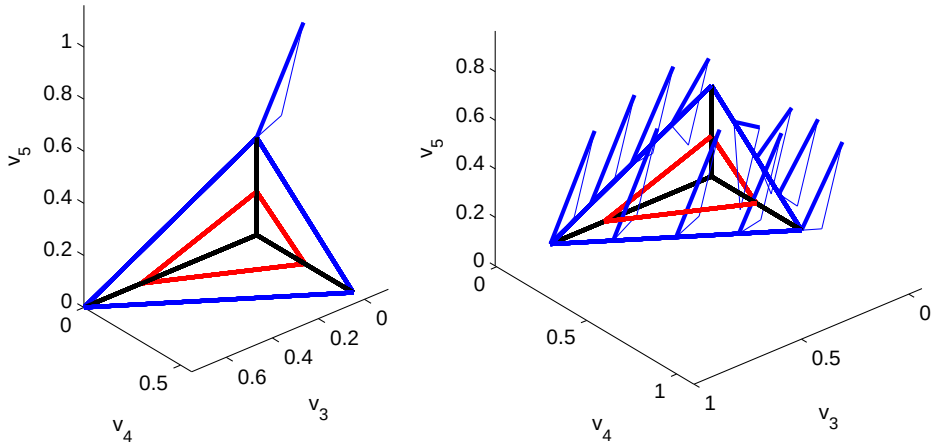

Figure 8: The linear (left) and nonlinear (right) gradients and their projections, for $c_A = 4.5$. In the right-side plot, the gradient at $v_5 = 3/8$ is nearly straight down the outer face, and is not shown. Gradients on the inner face point outward, and are not shown.

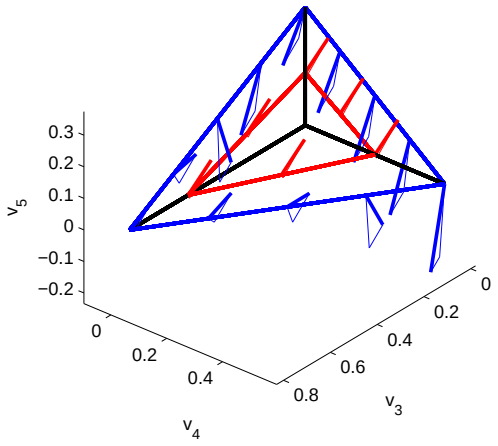

Figure 9: Gradients from the nonlinear analysis, and their projections, for $c_A = 3.9$.

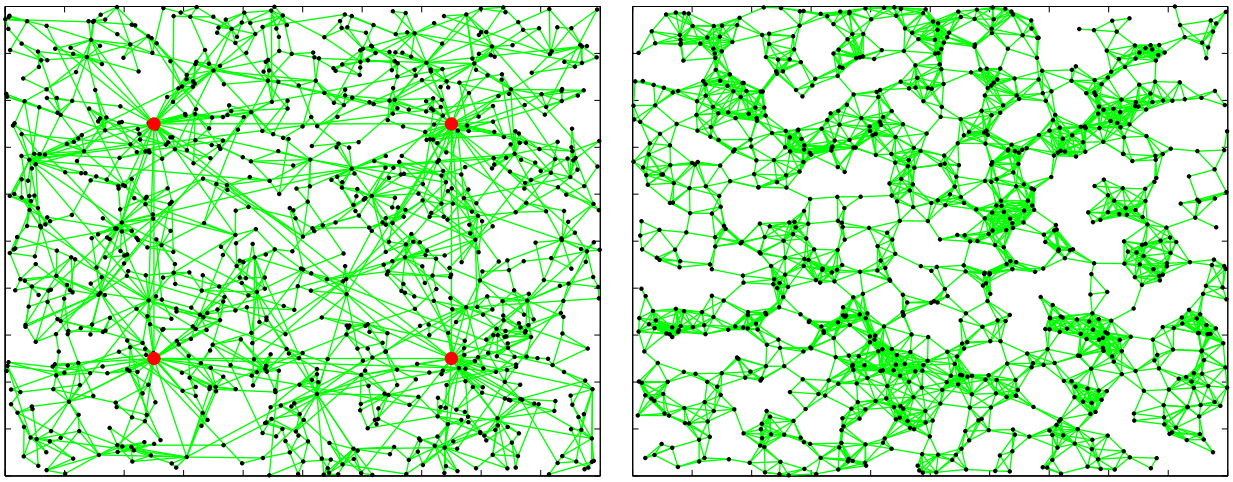

Figure 10: (Left) Layout of a typical hybrid geometric-scale-free graph, in which preferential attachment is enhanced by the geographic closeness of points. The four hubs shown are defined and connected at the first iteration. This realization has one thousand nodes and a mean degree of four. (Right) Layout of a typical geometric graph realization, with one thousand nodes on the unit square, threshold distance 0.054, and mean degree 8.8.

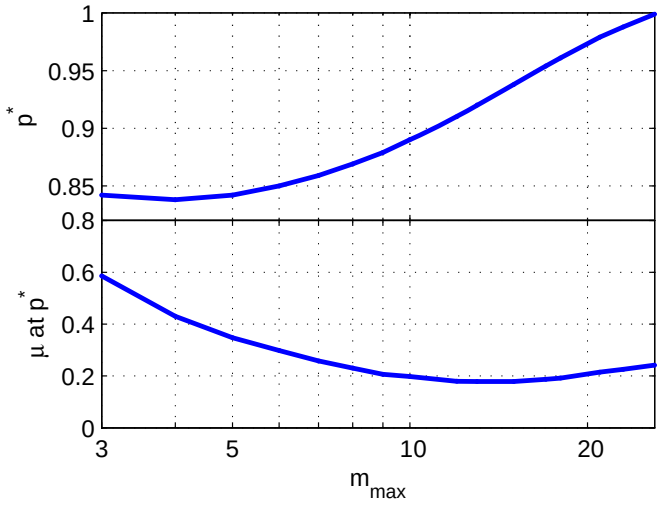

Figure 11: Asymptotic model p^* values for different split designs w satisfying $c_A = 2.5$, for the 4-SFPA on the B-side. In the split designs, node degrees are either one or approximately m_{max}.

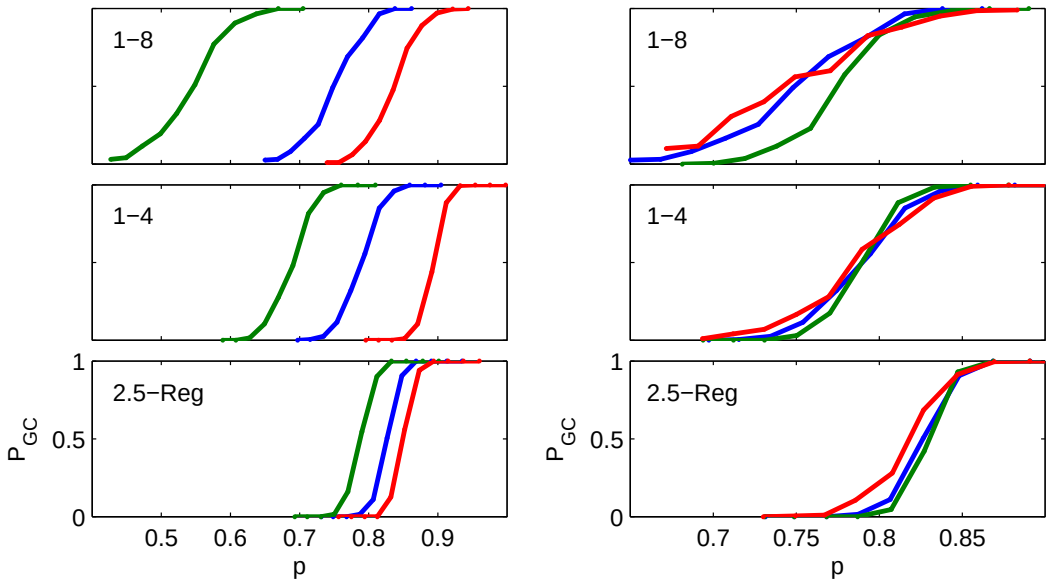

Figure 12: (Left) Giant component probability versus p for several A designs on for the 4-SFPA B-side, and $N = 1000$. Robustness differences are obtained via random (blue), matched (green), and inverse (red) ordering through the boundary between subsystems. p values corresponding with $P_{GC} = 0.50$ are approximately those given in Table 3. (Right) Effects of scale for the same structures, with random ordering only. The three curves for each degree distribution are for $N = 500$ (red), $N = 1000$ (blue) and $N = 2000$ (green). Note the change of horizontal scale; blue curves on both sides are identical.

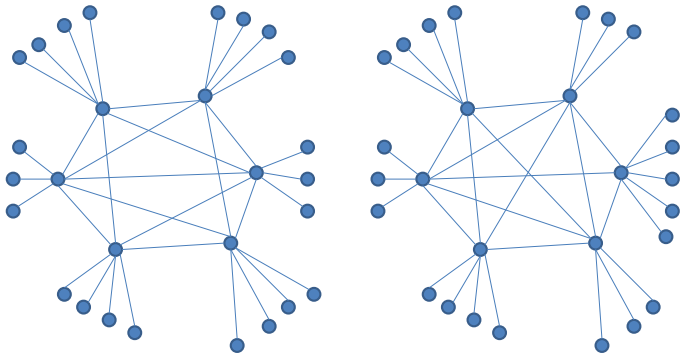

Figure 13: The two ways in which a 1-8 split design having mean degree 2.5 can be realized on 28 nodes, to isomorphism.

c_A-type	p^*	$p^* c_A$
γ_{ER}-ER	1^-	γ_{ER}
2.10-C Reg	0.995	2.09
2.20-C Reg	0.979	2.15
γ_{ER}-C Reg	0.913	2.24
2.70-C Reg	0.841	2.27
3.00-C Reg	0.759	2.28
4.00-C Reg	0.586	2.34
5.00-C Reg	0.475	2.38

Table 1: Robustness of paired regular random graphs. "ER" indicates Erdős-Rényi and "C Reg" indicates a regular random graph generated with the configuration model. $\gamma_{ER} = 2.4554$ (Buldyrev *et al.*, 2010)

	p	μ
$c_A = 3$	0.759	0.633
	0.800	0.766
	0.900	0.897
	0.950	0.950
$c_A = 4$	0.586	0.442
	0.600	0.510
	0.700	0.683
	0.800	0.797
	0.900	0.900

Table 2: Initial failure size applied versus final component size, for optimized paired regular random graphs. The first line for each c_A shows the minimum p (to three significant digits) that does not destroy the giant component, i.e., p^*.

	Inverse	Random	Matched
4-C Reg; 4-C Reg		0.576	
4-C Reg; 4-SFPA		0.600	
4-ER; 4-ER	0.712	0.606	0.513
4-SFPA; 4-SFPA	0.657	0.607	0.410
4-hgSFPA; 4-hgSFPA	0.741	0.697	0.566
8.8-geo; 8.8-geo	0.606	0.619	0.619
2.5-C SubOpt 1-8; 4-SFPA	0.835	0.748	0.549
L 2.5-C SubOpt 1-8; 4-SFPA		0.779	
2.5-C Opt 1-4; 4-SFPA	0.892	0.794	0.691
L 2.5-C Opt 1-4; 4-SFPA		0.791	
2.5-C SubOpt Reg; 4-SFPA	0.852	0.826	0.790
L 2.5-C SubOpt Reg; 4-SFPA		0.827	
2.5-C SubOpt 1-8; 4-hgSFPA	0.869	0.803	0.619
2.5-C Opt 1-4; 4-hgSFPA	0.905	0.827	0.726
2.5-C SubOpt Reg ; 4-hgSFPA	0.860	0.835	0.802
2.5-C SubOpt 1-12; 8.8-ER	0.631	0.507	0.415
2.5-C Opt 1-8; 8.8-ER	0.632	0.522	0.445
2.5-C SubOpt 1-4; 8.8-ER	0.663	0.618	0.565
2.5-C SubOpt Reg; 8.8-ER	0.727	0.718	0.704
2.5-C SubOpt 1-12; 8.8-geo	0.811	0.748	0.718
2.5-C Opt 1-8; 8.8-geo	0.779	0.748	0.741
2.5-C SubOpt 1-4; 8.8-geo	0.767	0.748	0.754
2.5-C SubOpt Reg; 8.8-geo	0.786	0.782	0.779

Table 3: Cascading failure results with 1000-node graphs; listed are the p-values for which half of the realizations collapse and the other half do not. The three data columns refer to connecting the A and B sides so that the node degrees are inversely correlated, randomly paired, or positively correlated. The upper grouping gives examples having a standard random graph on both the A and B sides; the lower grouping applies A-side optimized designs to specific B-side distributions. For each pairing, the A, B-side graph descriptions are separated by a semicolon; for each, the prefix (2.5, 4, or 8.8) indicates the mean degree, and the suffix is the structure. "C" indicates construction using the configuration model, "Reg" is a regular graph, "SFPA" is a scale-free graph using preferential attachment, "ER" is an Erdős-Rényi graph, "hgSFPA" is a hybrid geometric SFPA graph as described in the text, and "geo" is a geometric graph. "Opt" refers to an optimized split design using the asymptotic model; several suboptimal cases are given also. All runs are with $N = 1000$, except those with a leading "L", which have $N = 2000$.